

The impact of peripheral circulation characteristics of typhoon on sustained ozone episodes over the Pearl River Delta region, China

Ying Li^{1,2}, Xiangjun Zhao^{1,2,3}, Xuejiao Deng⁴, Jinhui Gao^{1,2,5}

¹ Department of Ocean Sciences and Engineering, Southern University of Science and Technology, Shenzhen, China

² Center for Oceanic and Atmospheric Science at SUSTech (COAST), Southern University of Science and Technology, Shenzhen, China;

³ School of Mathematics and Finance, Chuzhou University, Anhui 239000, China

⁴ Institute of Tropical and Marine Meteorology/Guangdong Provincial Key Laboratory of Regional Numerical Weather Prediction, China Meteorological Administration, Guangzhou, China

⁵ Plateau Atmosphere and Environment Key Laboratory of Sichuan Province, School of Atmospheric Sciences, Chengdu University of Information Technology, Chengdu, China.

Correspondence: Xiangjun Zhao (iamzxj841025@163.com) and Xuejiao Deng (dxj@gd121.cn)

Abstract. The peripheral circulation of typhoon forms sustained ozone episodes. However, how it impacts the day-to-day ozone pollution levels during the episodes has not been clearly studied, which is crucial for better prediction of the daily ozone variation. In this study, the analysis of ground observation, wind profile data, and model simulation are integrated. By analysing the wind profile radar observations, we found a weak wind deepening (WWD; vertical depth of the weak winds increased), more correlated with the ground-level ozone variation than surface weak wind. Long-term statistical analyses showed that the WWD is a common weather phenomenon in the peripheral subsidence region of typhoons and is generally accompanied by ozone pollution episodes. WRF-Chem with process analysis simulation showed that the peripheral subsidence chemical formation (CHEM) and vertical mixing (VMIX) effects are two major contributors to the enhancement of ozone levels to form the episode, while the advection (ADV) showed negative values. However, the day-to-day variation of the daytime ozone levels during the episode are not determined by the daily variation of daytime CHEM and VMIX, but dominated by the ADV terms. Therefore, the ozone and its precursors accumulation, including the enhancement during the nighttime, contribute to the daytime ozone increase in the following day. A detail day-to-day process analysis showed that in addition to decrease of negative ADV values (e.g. the weakened advection outflow or dispersion) on the ground, the integrated effect of the daily variation of the accumulative CHEM and ADV above the ground throughout the PBL determined together the overall day-to-day daytime ozone variation on the ground through the VMIX process. The results indicate that the peripheral characteristics of approaching typhoon not only form the ozone episode by the enhanced photochemical reactions but also could increase the day-to-day daytime ozone levels via pollution accumulation throughout the PBL due to the WWD up to 3-5 km. These results illustrate the important role of the WWD in the lower troposphere for the formation of sustained ozone episodes due to the peripheral circulation of the typhoon, which helps to better predict the daily changes of daytime ozone levels.

36 **1. Introduction**

37 The Pearl River Delta (PRD), located in the coastal region of South China and often affected by typhoon systems,
38 has experienced major economic development and urbanisation accompanied by large increase in air pollution and
39 decrease in visibility (Wang et al., 1998, 2001; Lai and Sequeira, 2001). Ozone pollution is the most significant air
40 pollution challenge in this region, and has been the ‘primary pollutant’ since 2014 (Ministry of Ecology and
41 Environment of China, 2016). Ozone is harmful to human health and has adverse effects on vegetation and crops,
42 among others (Aunan et al., 2000; Felzer et al., 2007; Feng et al., 2015). Ozone concentrations are determined by the
43 photochemical reactions of its precursors and local meteorological conditions. However, ozone pollution episodes are
44 mainly triggered by weather conditions rather than by sudden increases from emission sources (Ziomas et al., 1995;
45 Giorgi and Meleux, 2007; Lin et al., 2019; Li T. et al. 2018).

46 The Guangdong Haze Weather Bulletin (Wang, 2017) has classified the weather patterns affecting regional pollution
47 events into cold fronts, cold high-pressure systems moving towards the sea, uniform pressure fields, Western Pacific
48 subtropical high (WPSH), tropical cyclone (TC) peripheries, and weak cold high-pressure ridges. Using observational
49 data, several studies have reported the impacts of TC activity on meteorological factors that are favourable for air
50 pollution over the PRD region (Feng et al., 2007; Chen et al., 2008; Wu et al., 2013). TCs are typical weather systems
51 responsible for both high ozone and PM_{2.5} pollution over the PRD (Chen et al., 2008; Deng et al., 2019).

52 Previous studies in the PRD and other coastal regions of China have illustrated the significant impact of TCs on
53 forming ozone (TCs-Ozone) episodes (Zhang et al., 2012; Li et al., 2013, 2014; Zhang et al., 2013; Jiang et al., 2015;
54 Huang et al., 2015; Shu et al., 2016, 2019; Tan et al., 2018; Chen et al., 2018; Han et al., 2019). TCs-Ozone episodes
55 generally occur when weather conditions such as high temperatures, radiation flux, low relative humidity, and weak
56 wind (Cheng et al., 2016; Liu et al., 2017). Observational-based studies have reported that the TCs-Ozone episodes are
57 associated with weak wind, however the mechanism underlying the effect of weak wind on ozone in TCs-Ozone
58 episodes remains to be fully elucidated. In addition, previous process analysis based on numerical modelling

59 simulations have shown that the chemical (CHEM) and vertical mixing (VMIX) effects are two major contributors to
60 ozone episodes, whereas advective transport (ADV) is generally a consumptive process (Shu et al., 2016; Wang et al.,
61 2009). The inconsistencies between observational and simulated results of wind contributions to ozone episodes are
62 poorly understood, which may be attributed to the limited data on the influence of weak wind on ozone concentration
63 enhancement.

64 In addition, for the air quality forecast and prevention, it is important to understand the mechanism underlying the
65 day-to-day variation of the daytime ozone levels, since the ozone levels peak during the daytime due to photo-chemical
66 effects; ozone is converted to NO₂ temporarily in the absence of light (Li Y. et al. 2012). However, though the
67 TCs-Ozone episodes have been widely reported, the studies of mechanism on the daily daytime variation of during
68 sustained TCs-Ozone episodes are limited.

69 Thus, the objective of this study is to understand the impact processes of typhoon circulation characteristics on the
70 day-to-day variation of daytime ozone concentration in TCs-ozone episode. The analysis of ground observation, wind
71 profile data, and WRF-Chem model simulation with process analysis are integrated. Detailed data and model
72 description are provided in Section 2, followed by the results and discussion in Section 3. The main conclusions are
73 summarized in Section 4.

74 **2. Data and model**

75 **2.1 Data**

76 In this study, hourly surface ozone concentrations from 2016 over mainland China were obtained from the Ministry of
77 Environmental Protection of China. The 3D wind profiler data, automatic weather station data, cloud data, and solar
78 radiation measurements were provided by the China Meteorological Administration and were used for the
79 meteorological analyses of Typhoon Nepartak. The Final (FNL) Operational Global Analysis data used to describe the
80 circulation of Typhoon Nepartak have a horizontal resolution of 1° x 1° with 27 vertical levels and were obtained from
81 the National Centers for Environmental Prediction (NCEP), USA .

82 The observations of a typical ozone episode occurred in the PRD region during 7–10 July 2016 (local standard time;
83 LST) before Typhoon Nepartak made landfall was collected and analysed. Typhoon Nepartak intensified into a super
84 typhoon at 20:00 on 5 July, then gradually moved northwest due to the forcing of the WPSH over its northeastern side
85 (Fig. S2). At 05:50 on 8 July, the typhoon made landfall in Taitung County, Taiwan, with a maximum wind speed of 60
86 m s^{-1} , and again in Shishi City, Fujian at 14:00 on 9 July, with a maximum wind speed of 23 m s^{-1} . At 03:00 on 10 July,
87 the typhoon weakened into a tropical depression.

88

89 **2.2 Model descriptions**

90 WRF-Chem is a widely used and fully coupled online 3D Eulerian chemical transport model
91 (<https://ruc.noaa.gov/wrf/wrf-chem/>) that considers both chemical and physical processes (Zhang et al., 2010; Forkel et
92 al., 2012); version 3.9.1.1 was applied in this study. Detailed descriptions of the meteorological and chemical aspects
93 of the WRF-Chem model have been previously reported by Grell et al. (2005) and Skamarock et al. (2008). For the
94 simulation, two nested domains (Fig. S1) were set up with horizontal resolutions of 27 and 9 km and grids of $283 \times$
95 184 and 223×163 for the parent domain (D1) and nested domain (D2), respectively. D1 was centred at (28.5°N ,
96 114.0°E) covering most of China, the surrounding countries, and the ocean. Corresponding simulations provided
97 meteorological and chemical boundary conditions for D2, which covered most of southern China.

98 There were 39 vertical layers that extended from the surface up to a pressure maximum of 50 hPa, 12 of which were
99 located in the lowest 2 km to fully describe the vertical structure of the PBL. Carbon Bond Mechanism Z (CBM-Z),
100 which includes 133 chemical reactions for 53 species and extends the model framework to function for a longer time
101 period and at a larger spatial scale than its predecessor, was used as the gas-phase chemical mechanism (Zaveri and
102 Peters, 1999). The corresponding aerosol chemical mechanism was the Model for Simulating Aerosol Interactions and
103 Chemistry (MOSAIC) with eight bins (Zaveri et al., 2008), which is extremely efficient and does not compromise
104 accuracy of the aerosol model calculations. Other major model configuration settings are listed in Table 1.

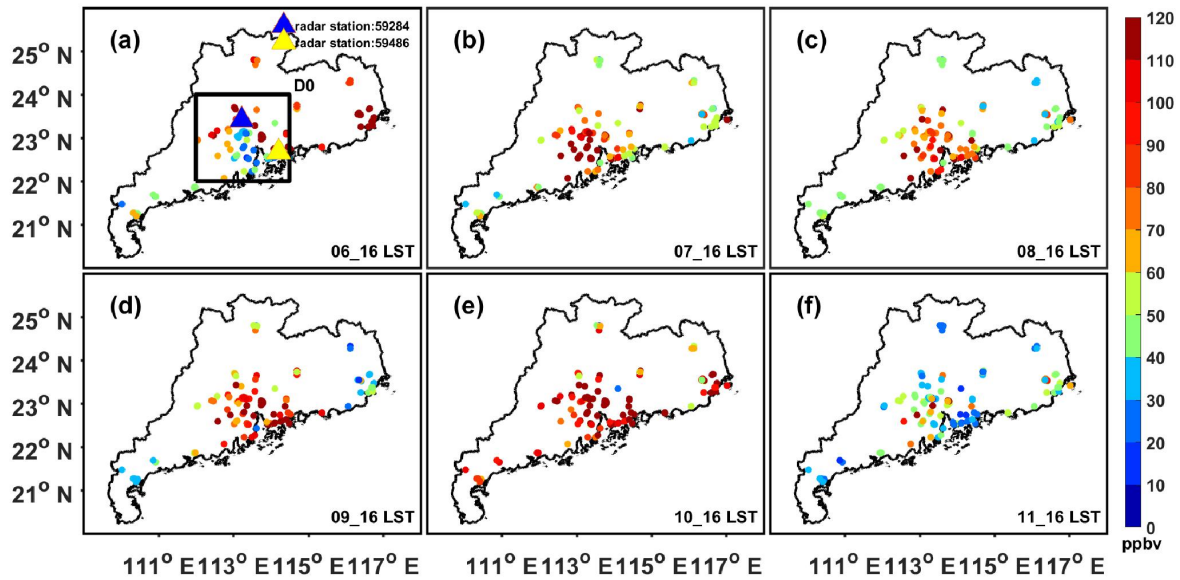
105 **Table 1.** Major model configuration options used in the simulations.

| ITEM | Selection |
|-----------------------|--------------------------------|
| Long wave radiation | RRTMG |
| Shortwave radiation | RRTMG |
| Microphysics scheme | Lin scheme |
| Boundary layer scheme | Yonsei University (YSU) scheme |
| Land surface option | Noah land surface model |
| Photolysis scheme | Fast-J photolysis |
| Dry deposition | Wesely scheme |

106 3. Results and discussion

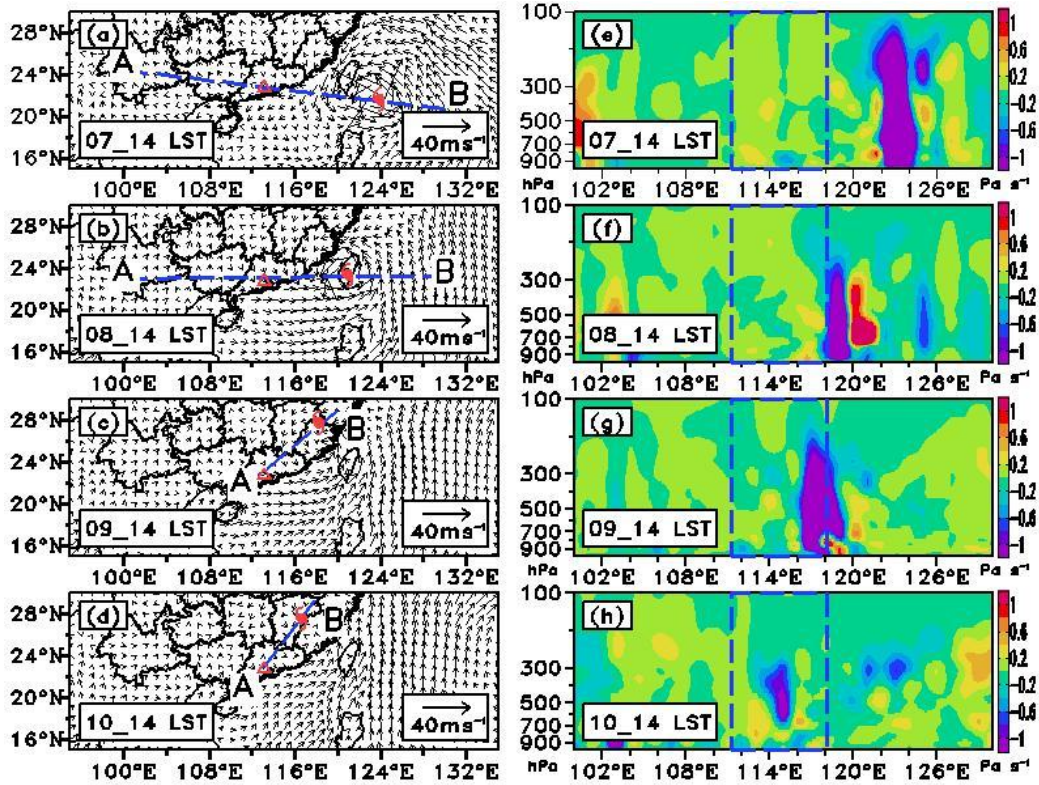
107 3.1 Episodic data analysis

108 The ozone pollution level and the meteorological conditions of the typhoon Nepartak case was first analysed. As
109 shown in Fig. 1, Guangdong province experienced a severe ozone pollution during the period 7-10 July; from 28% (July
110 7) to 57% (July 10) of the air quality stations in Guangdong Province exceeded the national air quality standard
111 level-II for ozone ($200 \mu\text{g m}^{-3}$) at the daily peaks (16:00 LST). To show the vertical motion of the typhoon centre and
112 peripheral region, we constructed a cross section through the typhoon system (points A and B; Fig. 2a-d) and plotted
113 the corresponding vertical velocities (Fig. 2e-h) using the NCEP data. As shown in Fig. 2e-f, the western subsiding
114 branches of vertical typhoon circulation were located over the PRD during the 7th and 8th of July, when ozone
115 concentrations increased significantly compared to those of July 6. After Typhoon Nepartak made landfall at Shishi
116 City on July 9, the peripheral subsidence had moved to the western area of the PRD region (Fig. 2g-h) and the PRD
117 region was influenced by weak vertical motion and a weak horizontal wind field. Peak ozone levels exceeded 100 ppb
118 at most of the monitoring stations in the PRD at this time. On July 11, Typhoon Nepartak dissipated and the surface
119 ozone concentrations began to decrease (Fig. 1f).



120

121 **Figure 1.** The horizontal distribution of surface ozone concentration over PRD at 16:00 from (a) 6 July 2016 to (f) 11 July 2016. The
 122 yellow and blue triangles in (a) denote the positions of wind profiler station 59486 and 59284. The black box D0 indicates the area where
 123 the severe ozone pollution event occurred.

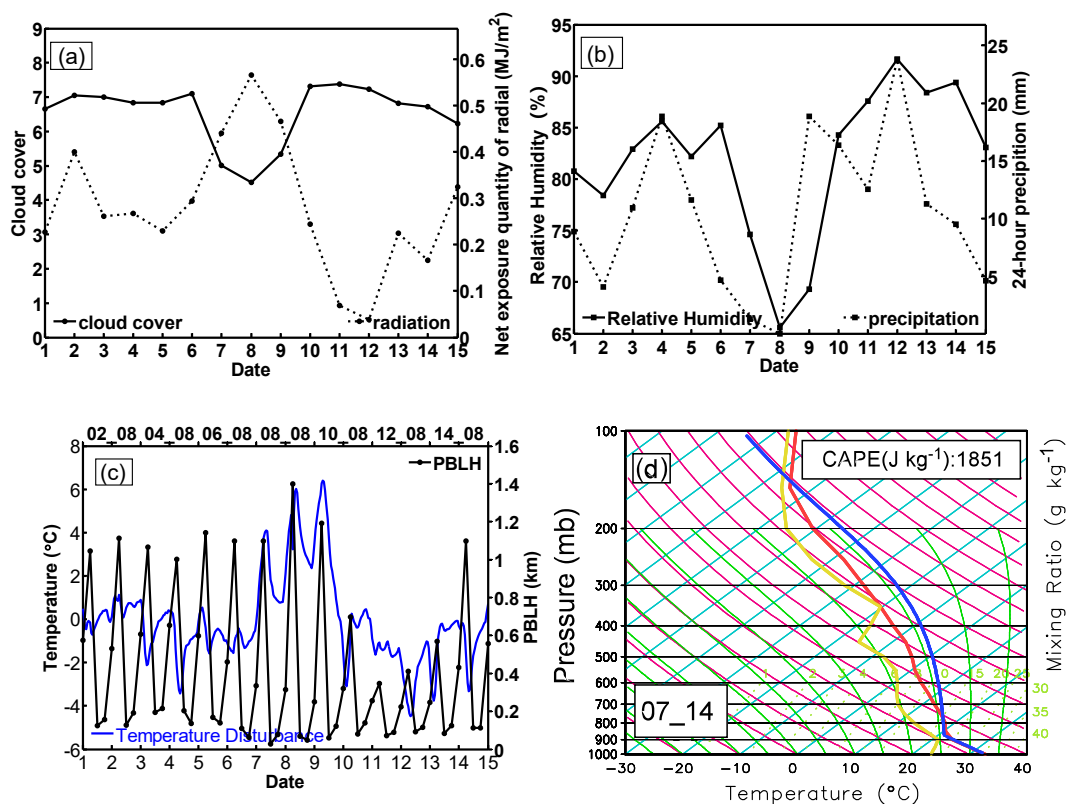


124

125 **Figure 2.** (a)-(d) 1,000 hPa wind vectors of NCEP-FNL data from 14:00 (July 7) to 14:00 (July 10) with red triangle and typhoon signs
 126 representing PRD centre and Nepartak locations, respectively. (e)-(h) vertical cross sections of vertical velocity along the four straight lines
 127 linking PRD and the centres of Typhoon Nepartak in (a)-(d) from 14:00, 7 July, to 14:00, 10 July of 2016. The four blue dashed boxes
 128 denote the longitude range of PRD in (e)-(h).

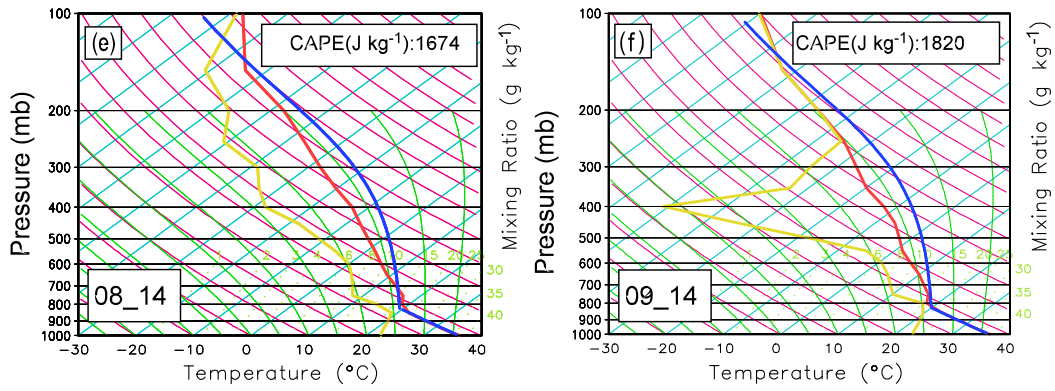
129 The weather over the PRD region was characterized as clear sky, strong solar radiation (Fig. 3a), low relative
 130 humidity (Fig. 3b), and high temperatures (Fig. 3c), when the subsiding branches of vertical typhoon circulation were

131 located over the PRD during the 7th and 8th of July (Fig. 2e-f). The variations in these surface meteorological variables
 132 exhibited favourable conditions for increasing ozone concentrations (Cheng et al., 2016; Liu et al., 2017). However,
 133 the height of the PBL increased significantly on 8th and 9th of July (Fig. 3c), and the atmosphere was under unstable
 134 conditions, which was indicated by the comparison between the adiabatic lapse rate (blue) and the environmental lapse
 135 rate (red) (Fig. 3d-f). This instability is also shown by the large values of convective available potential energy (CAPE;
 136 Fig. 3d-f), which is another criterion used to determine the stability of atmosphere. When the CAPE is $\sim 1,000 \text{ J kg}^{-1}$,
 137 the state of atmosphere is unstable, which is favourable for thermal convection. These results illustrate that, under the
 138 control of typhoon periphery, the PBL height can be increased in unstable atmospheric conditions, which is opposite
 139 from the observations in some TCs-haze events reported in previous studies (Wu et al., 2005 and Feng et al., 2007).
 140 For example, Wu et al.(2005) reported that the TC produces a strong descending motions in the lower troposphere, a
 141 weak surface wind speeds, and a lower PBL. Our results indicated that the TCs-Ozone episodes are not dependent on
 142 or necessarily associated with the enhancement of atmospheric thermal-dynamical stability and/or reduction of the
 143 PBL.



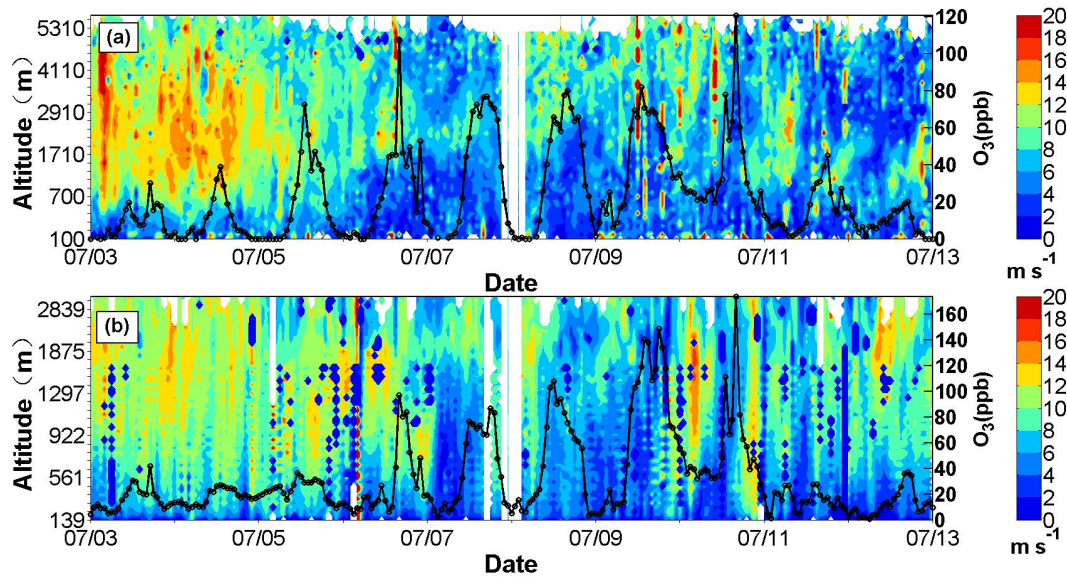
144

145



146
 147 **Figure 3.** Time series of diurnal mean (a) cloud cover, radiation at 59287 observation station, (b) relative humidity, 24-h
 148 precipitation and averaged (c) PBLH and temperature anomaly of region D0 from July 1 to 15; The SkewT/LogP at 14:00 on July 7 (d), 8
 149 (e) and 9 (f); the solid thick red, blue and yellow lines in d,e and f denote the temperature sounding, the parcel path from surface upward
 150 and the dewpoint sounding, respectively.

151
 152 The evolution of the vertical profile of horizontal winds at representative station 59284 is shown in Fig. 4a. Before
 153 July 5, the wind speed increased with the vertical atmospheric layers. There were relatively larger wind speeds above
 154 the PBL and weaker wind speeds below ~700 m, with relatively low surface ozone concentrations (< 40 ppbv). On
 155 July 5, the daily ozone concentration started to increase (> 70 ppbv) as the depth of WWD increased. The depth of
 156 WWD was ~3 km during July 7–9 with a sustained increase in ozone peak. On the night of July 11, the horizontal wind
 157 speed above ~1 km significantly increased while the ozone concentration decreased. Variations in the wind profile and
 158 surface ozone at another representative station are also shown in Fig. 4b. At this station, the depth of WWD started to
 159 increase on July 7, with a gradually increase in ozone peak value. Co-variations of the ozone concentration and WWD
 160 at other radar stations were also observed (Figs. S3–5). This co-variation is not a local effect, but a regional
 161 phenomenon.



162

163 **Figure 4.** The profile evolution of horizontal wind speed from July 3 to 13. The black solid lines are the surface ozone concentrations at (a)

164 59284 and (b) 59486 wind profile radar station.

165 By analysing the wind profile data (Fig. 4), we observed that the vertical depth of the horizontal weak wind generally

166 increased from the surface up to the lower troposphere (~2–3 km) and the surface ozone concentration changed with

167 the vertical depth of the horizontal weak wind. To further illustrate the different impact of the surface weak wind and

168 the WWD on surface ozone concentrations, the correlation coefficients between the surface ozone concentrations and

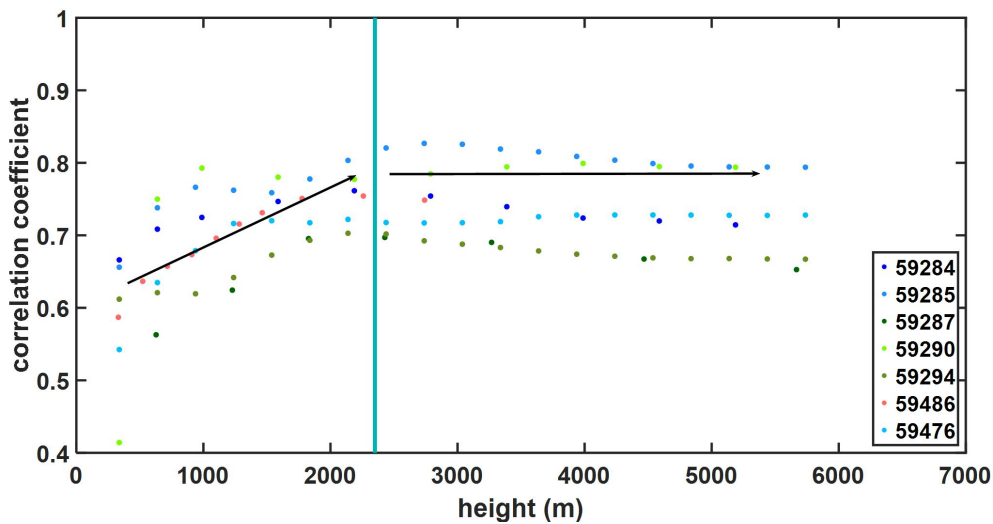
169 the average wind speeds from surface to different altitudes (up to 6 km) at different radar stations were calculated (Fig.

170 5). The correlation coefficients showed an increasing trend with altitude, reaching maximum values between 2–3 km

171 and remained stable at above ~2.5 km. The average correlation coefficient at the surface was 0.57 (0.41–0.67) and the

172 average correlation coefficient above 2,000 km was ~0.75 (0.69–0.83) for seven radar stations. This indicates the

173 potential impact of WWD on the ozone pollution episode induced by Typhoon Nepartak.



174

175

Figure 5. Correlation coefficient between the evolution of average wind speed and the evolution of ground ozone concentration in different altitude ranges of each wind profile radar station.

176

177

3.2 Long-term statistical analysis of the relationship between WWD and the ozone episode

178

Long-term statistical analysis showed no stable atmospheric stratification and a decrease in the height of the boundary

179

layer in this ozone pollution episode. The analysis of wind profile radar data and the correlation coefficients between

180

the surface ozone concentrations and the average wind speeds between the surface and the altitude of each vertical

181

layer (up to 6 km) indicated that in this episode of ozone pollution, WWD might have played an important role in the

182

increasing of ozone pollution at the surface. The Guangdong Province is located on the western coast of the Pacific

183

Ocean and is frequently affected by typhoons. To investigate whether the relationship between WWD and ground-level

184

O₃ only occurred in this case study or is a common phenomenon, a long-term statistical analysis of historical data was

185

conducted. A statistical analysis of tropical cyclone wind fields in the Northwestern Pacific Ocean from 2014 to 2018

186

(based on Guangdong wind profiler data) was conducted. As not all the radar stations in Guangdong province are

187

available during a typhoon, the available statistics number of each radar station for the 38 typhoons were recorded as

188

M. The number of WWD instances at each radar station was recorded as n. Ozone concentrations above 100 $\mu\text{g m}^{-3}$ are

189

harmful to human health (Organization, 2005).

190

The PRD regional background ozone concentration is generally less than 80–100 $\mu\text{g m}^{-3}$ and the ozone concentrations

191

at most stations can exceed 160 $\mu\text{g m}^{-3}$ (national AQ standard Level-I) during a regional ozone pollution event.

192

Therefore, ozone concentrations of 100–160 $\mu\text{g m}^{-3}$ and above 160 $\mu\text{g m}^{-3}$ were used to denote regional light and heavy

193 ozone pollution in the statistics. The numbers of regional light and heavy ozone pollution events at each radar station
 194 were recorded as n_1 and n_2 , respectively. As shown in Table 2, the number of WWD occurrences (n) accounts for
 195 87–97% of the available number(M) of radar stations in the 38 typhoon statistics for the seven radar stations. The
 196 average value of n/M for the seven radar stations is 93%. This indicates that, when there is a tropical cyclone in the
 197 Northwestern Pacific Ocean, WWD occurs in whole or part of Guangdong province. The number of ozone pollution
 198 occurrences (n_1+n_2) accounts for 78%-100% of the number of WWD occurrences(n). The average value of $(n_1+n_2)/n$
 199 for the seven radar stations is 94%. The above statistical results show that WWD may be a common phenomenon on
 200 the periphery of typhoons and is often accompanied by significant increases in ozone concentrations.

201 Table 2. The statistical results of the peripheral weak wind of 38 tropical cyclones for 7 radar stations in Guangdong

202 Province and ozone concentration from 2014 to 2018.

| Radar station number | n/M^a | $(n_1 + n_2)/n^b$ |
|----------------------|---------------|-------------------|
| 59294 | 33/38 (87%) | (21+11)/33 (97%) |
| 59486 | 32/33 (97%) | (18+12)/32 (94%) |
| 59476 | 29/30 (97%) | (22+5)/29 (93%) |
| 59285 | 33/36 (92%) | (21+12)/33 (100%) |
| 59287 | 35/38 (92%) | (23+12)/35 (100%) |
| 59284 | 24/25 (96%) | (19+5)/24 (100%) |
| 59290 | 28/30 (93%) | (13+9)/28 (78%) |
| Ave. | 93% (87%-97%) | 94%(78%-100%) |

203 ^a n/M represents the percentage of the number of WWD occurrences in the effective observation number of radar station
 204 in 38 typhoons.

205 ^b $(n_1+n_2)/n$ represents the percentage of the number of ozone pollution occurrences in the number of WWD occurrences
 206 in 38 typhoons.

207 The above correlation coefficients and statistical analysis indicate that WWD may be a common weather
 208 phenomenon in the periphery of typhoon and could impact the ground-level ozone concentration. In the subsequent

209 section, the influence of WWD on ground-level ozone pollution and the impact of typhoon peripheral circulation on
210 sustained ozone enhancement during Typhoon Nepartak are discussed based on WRF-chem numerical simulation.

211 **3.3 Model simulation and validation**

212 To investigate the impact of typhoon periphery and WWD on formation of the sustained ozone episode, the numerical
213 model with the process analysis was applied, prior to which the model performance was validated using the available
214 observations. Figure S6a-d presents the measured and simulated data for temperatures, wind speeds, wind directions,
215 and ozone concentrations at Guangzhou from 00:00 on July 3 to 07:00 on July 15 of 2016. With regards to the
216 meteorological variables, there was good agreement between the measured and modelled results, especially the shifting
217 wind features, implying that the model successfully captured the synoptic features. However, ozone concentrations
218 (Fig. S6d) overestimated low values or underestimated high values. However, the simulated results and observed data
219 reasonably agreed with each other and captured the ozone episode in the region.

220 Statistical metrics including the index of agreement (IOA), mean bias (MB), root mean square error (RMSE), and
221 normalised mean bias (NMB) were used to further assess the model performance (Table 3). The IOA of the wind
222 direction was determined according to Kwok et al. (2010), while the IOA values for the other variables were calculated
223 as per Lu et al. (1997). Our simulation of the time series of ozone concentrations and meteorological variables was
224 reasonable. All the meteorological parameters were close to the corresponding simulation results in the PRD region
225 (Wang et al., 2006; Li et al., 2007; Hu et al., 2016). IOAs for temperature and wind speed (0.89 and 0.66, respectively)
226 reached the criteria (as presented in the brackets of Table 3). The model performed well at capturing the wind
227 directions, with a small MB of 7.72°. MBs and NMBs for temperature and wind speed exceeded the benchmarks, and
228 were comparable to the findings of Li et al.(2013) with a slight overestimation, which is probably due to the
229 incomplete resolution of the urban morphology impact in the model (Chan et al., 2013).

230 Moreover, ozone concentrations are well simulated, with an IOA of 0.84 and an NMB of 4.83. Time series
231 comparisons of ozone concentrations and meteorological factors at Shenzhen, Zhongshan and Zhuhai are presented in

232 Figs. S6a1-d1, a2-d2 and a3-d3. The overall results suggest that the model could reproduce ozone concentrations and
233 capture the transport features in southern China.

234 **Table 3.** Statistical comparison between the observed and simulated variables. The benchmarks are based on
235 Emery et al.(2007) and EPA (Doll, 1991).

| Variable ^a | IOA ^b | MB ^b | RMSE ^b | NMB ^b (%) |
|----------------------------|------------------|-----------------|-------------------|----------------------|
| Temp (°C) | 0.89 (≥0.8) | 0.75 (≤±0.5) | 1.90 | 2.68 |
| Wspd. (m s ⁻¹) | 0.66 (≥0.6) | 0.65 (≤±0.5) | 1.45 (≤±2.0) | 37.81 |
| Wdir. (°) | 0.77 | 7.72 (≤±10) | 85.88 | 4.24 |
| Ozone (ppbv) | 0.84 | 9.53 | 37.15 | 4.83 (≤15) |

236 Values that did not reach the criteria are indicated in grey.

237 ^a Temp. = temperature; Wspd. = wind speed; Wdir. = wind direction.

238 ^b IOA is the index of agreement; MB is the mean bias; RMSE is the root mean square error; NMB is the normalized mean bias.

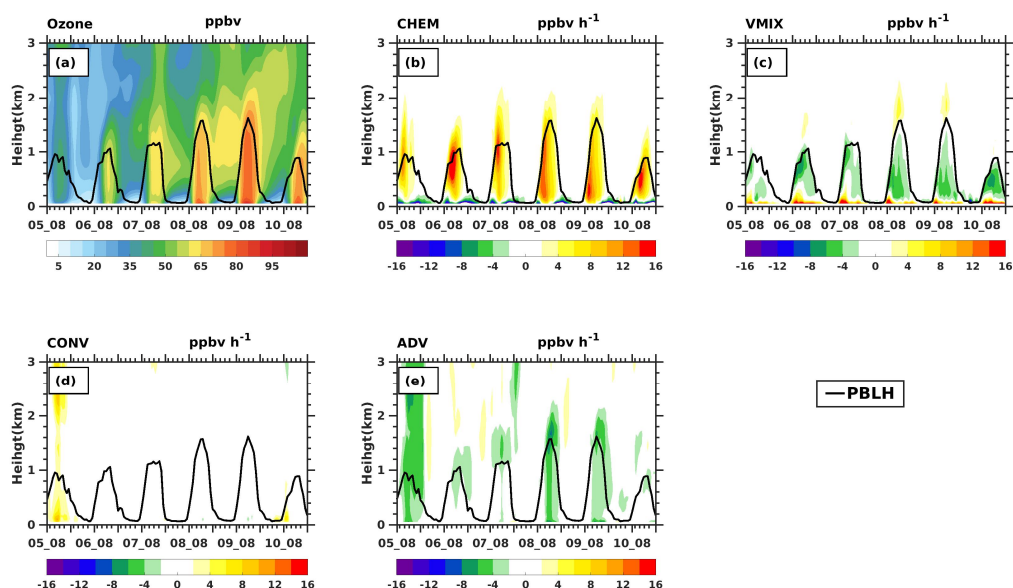
239 **3.4 Process analysis of the impact of typhoon peripheral circulation on sustained ozone** 240 **enhancement and influence mechanism of WWD on ground-level ozone**

241 Variations in ozone concentration are directly caused by physical and chemical processes (Zhu et al., 2015), the fact
242 that peripheral circulation of a typhoon affects ozone concentration can be discussed using an process analysis. The
243 following processes were considered in this analysis: (1) advective transport (ADV), which is strongly related to wind
244 and ozone concentration gradients from upwind areas to downwind areas; (2) vertical mixing (VMIX) caused by
245 atmospheric turbulence and vertical gradients of ozone concentrations, which are related to variations in the PBL
246 (Zhang and Rao, 1999; Gao et al., 2017); (3) chemistry (CHEM), which is the result of chemical calculations that
247 include ozone chemical production and consumption; (4) convective processes (CONV), i.e., the ozone contribution
248 due to convective movements. Complete details on the analytical process of the WRF-Chem model are described in
249 previous studies (J. Gao et al., 2016; H. Zhang et al., 2014) and in the WRF-Chem user guide.

250 Figure 6a shows the profile evolution of the average ozone concentrations in region D0 (black box D0 in Fig. 1)
251 from 08:00, on July 5, to 20:00, on July 10. The ozone concentrations gradually increased from July 6-9 throughout the
252 PBL, with an increase in PBL height of up to ~1.5 km. On July 10, the PBL height decreased to less than 1 km, while
253 the ozone concentration decreased with PBL; however, it remained high, yet lower than that on July 9. Figure 6b-e

254 show the vertical distributions of the processes that contribute to the ozone concentrations.

255 It can be seen from Fig. 6b-e, during the period from 08:00 to 20:00 on July 5-10, the contributions of CONV in PBL
256 were zero; CHEM on the ground showed strong negative contributions, and VMIX on the ground showed strong
257 positive contributions; ADV in PBL showed weak negative contributions during July 6 and 7, and the negative
258 contributions of ADV in PBL were strengthened on July 8 and 9. Therefore, the contributions of ground VMIX and
259 CHEM played a major role in the change of the PBL ozone concentrations, which is consistent with previous studies in
260 the PRD region (Wang et al. 2009). The enhanced ozone above ground due to the CHEM effect contributed to the
261 ground ozone enhancement through the increased VMIX effect. At the same time, changes in the strength of ADV
262 contributions in PBL might also have a certain impact on the changes in the ozone concentrations on the ground.



263
264 **Figure 6.** The profile evolution of averaged (a) ozone concentration and (b)-(e) CHEM, VMIX, CONV, and ADV of region D0 from 08:00,
265 July 5, to 20:00, July 10. The black lines denote the planetary boundary layer height (PBLH).

266 In order to investigate the cause of the continued day-to-day increase of the daytime ozone concentration during the
267 sustained ozone episode, the numerical relationship between the daytime (we used 08:00 to 20:00 in this study)
268 average ozone concentration difference of two adjacent days and the various physical and chemical processes must be
269 quantified. Based on the numerical process analysis, the difference between the daytime average ozone concentrations
270 on two adjacent days (DDOC) can be further expressed by accumulative contribution between the periods, which can

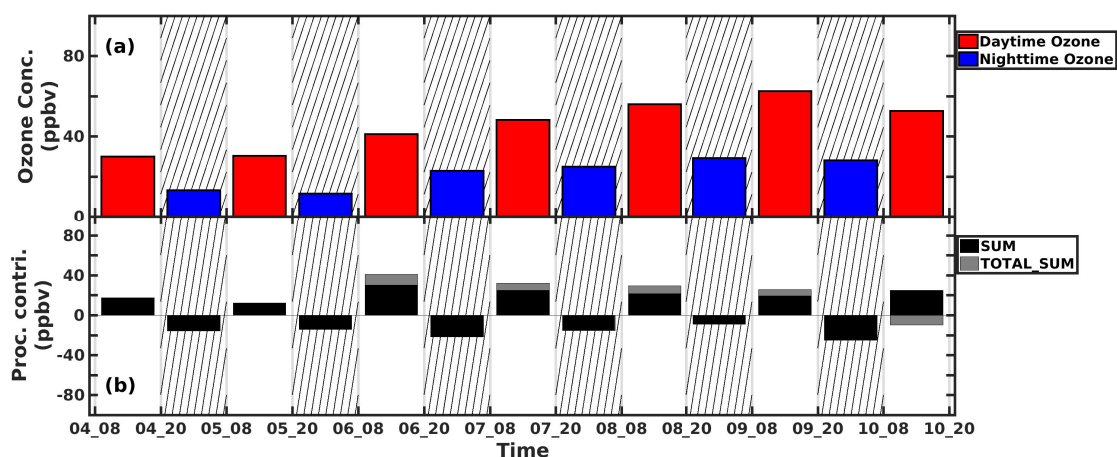
271 be expressed into three continuous contribution terms:

$$272 \quad C_{d2} - C_{d1} = \frac{1}{N} \sum_{t1=09}^{t1=20} (t1 - 8) \cdot \text{SUM}_{t1} + \sum_{t2=21}^{t2=08} \text{SUM}_{t2} + \frac{1}{N} \sum_{t3=09}^{t3=20} (21 - t3) \cdot \text{SUM}_{t3}, \quad (1)$$

273 where C_{d2} and C_{d1} are the daytime average ozone concentrations on two adjacent days (see SI for detailed
274 derivation). N is the total number of time slots for the daytime period between 08:00-20:00. When the right side of Eq.
275 (1) > 0 , the daytime average ozone concentration will increase compared to the daytime average concentration from
276 the previous day, and vice versa. The three terms on the right side of Eq. (1) are referred to as $\text{SUM}_{d,d1}$, $\text{SUM}_{n,d1}$, and
277 $\text{SUM}_{d,d2}$, respectively. $\text{SUM}_{d,d1}$ and $\text{SUM}_{d,d2}$ reflect the daytime contributions on two adjacent days. $\text{SUM}_{n,d1}$ reflects
278 the nighttime contribution between the two adjacent days. Therefore, the DDOC is determined by the sum of these
279 three terms, which we referred to it as TOTAL_SUM . According to Eq. (1): TOTAL_SUM is consistent with the
280 evolution of daytime average ozone concentration, that is, when $\text{TOTAL_SUM} > 0$, daytime average ozone
281 concentration increases; when $\text{TOTAL_SUM} < 0$, daytime average ozone concentration decreases. It can be seen from
282 Fig. 7, during the daytime of July 6-9, TOTAL_SUM was positive, and the corresponding daytime average ozone
283 concentrations gradually increased; meanwhile, on July 10, TOTAL_SUM was negative, and daytime average ozone
284 concentration began to decrease. The daytime SUM on July 10 remained positive. The above analyses indicate that
285 TOTAL_SUM can well reflect the changing trend of DDOC, therefore the cause of the daily daytime ozone variation
286 during sustained episode can be analysed according to Eq. (1).

287 Notably, the ozone chemistry between the daytime and nighttime is different. The SUM value during daytime is always
288 positive while the SUM of the nighttime is always negative. In terms of the daily daytime variation, the separated three
289 terms of TOTAL_SUM reveals that the daily variation of daytime ozone level not only determined by the daytime
290 chemistry but also influence by the nighttime ozone variation between the two adjacent days. For example, the
291 nighttime consumption or accumulation of ozone (as well as precursors) could contribute to the daytime ozone
292 increase of the following day; therefore, in diagnostic forecasting of daily air quality, an increase in daytime ozone
293 level can be expected, if the concentration of ozone precursors enhanced in the previous night but the meteorological

294 condition remains unchanged between the two adjacent daytimes.



295
296 **Figure 7.** (a) daytime and nighttime ozone concentrations and (b) SUM and TOTAL_SUM on the ground within region D0 during 08:00,
297 July 4, to 20:00, July 10.

298 Table 4. The decomposed accumulative CHEM, VMIX, CONV and ADV effects of the TOTAL_SUM on the
299 ground.

| Period | | | | | | |
|---------------|-----------|-----------|---------------|-----------|-----------|------------|
| (ppbv) | 4_08-5_20 | 5_08_6_20 | 6_08-7_20 | 7_08-8_20 | 8_08-9_20 | 9_08-10_20 |
| TOTAL_SUM | | | | | | |
| _CHEM | -138.16 | -113.82 | -133.38 | -96.68 | -75.12 | -133.96 |
| TOTAL_SUM | | | | | | |
| _VMIX | 118.85 | 113.40 | 131.09 | 88.91 | 70.38 | 105.23 |
| TOTAL_SUM | | | | | | |
| _CONV | 33.70 | 13.50 | -1.73 | 0.81 | -2.72 | 12.13 |
| TOTAL_SUM_ADV | | | | | | |
| | -13.96 | -3.31 | 10.97 | 15.06 | 14.01 | 6.91 |
| TOTAL_SUM_CVC | | | | | | |
| | 14.39 | 13.089 | -4.01 | -6.96 | -7.45 | -16.60 |
| TOTAL_SUMs | 0.4242 | 9.7734 | 6.957 | 8.1045 | 6.5583 | -9.6872 |

300 The highlighted column indicates the non-attainment (national-II air quality standard) ozone period.
301 TOTAL_SUM_CAC is the sum of the TOTAL_SUM_(CHEM+VMIX+CONV).

302 Further, DDOC or TOTAL_SUM of two adjacent daytimes can be decomposed into contributions of the different
303 processes (CHEM, VMIX, CONV, ADV). We name the four accumulative terms as TOTAL_SUM_CHEM,
304 TOTAL_SUM_VMIX, TOTAL_SUM_CONV and TOTAL_SUM_ADV accordingly (see Eq.(5) in SI for details). The

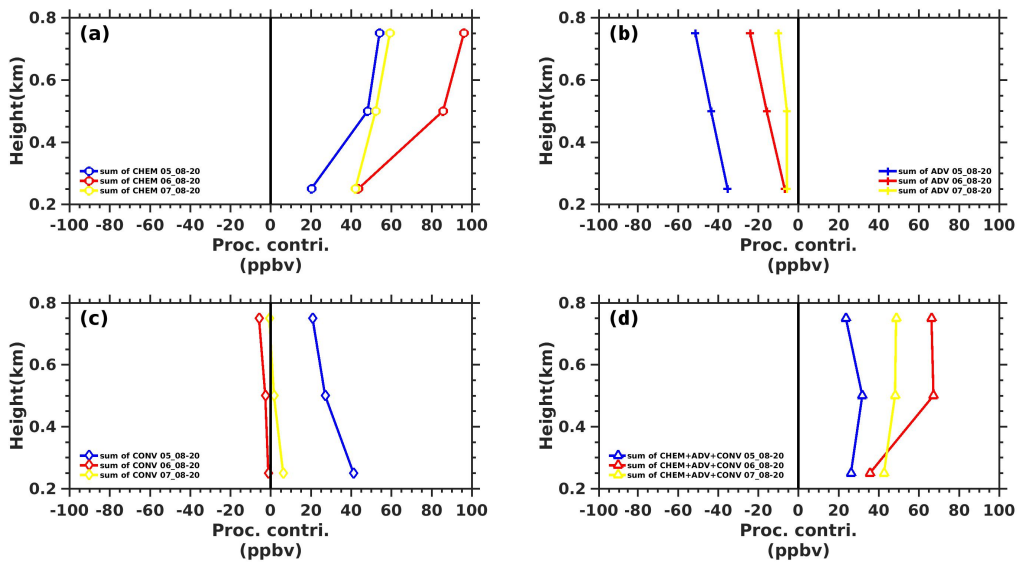
305 details budget of the TOTAL_SUM_CHEM, TOTAL_SUM_VMIX and TOTAL_SUM_CONV during the episode
306 between two adjacent daytimes are presented in Table 4. Each column shows an accumulative contribution of different
307 process from 08:00 to 20:00 of the next day. The results show that both the VMIX and ADV enhancement contributed
308 to the daily increase of daytime ozone concentration from July 6 to 9 on the ground. More specifically, during the
309 episode (columns highlighted by brown colour), the TOTAL_SUM_VMIX contributions are always positive on the
310 ground and reach maximum from July 6 to 7, while the TOTAL_SUM_CHEM contributions are negative, which
311 should be the result of the surface NO-titration effect. The TOTAL_SUM_CONV contributions are relatively ignorable,
312 while the TOTAL_SUM_ADV contributions significantly increased from negative value to positive value during the
313 episode period. Since the CHEM and VMIX are significantly associated with each other, the combined contribution of
314 CHEM, VMIX, and CONV to the TOTAL_SUM is shown by the TOTAL_SUM_CVC in the Table 4. The
315 CHEM+VMIX+CONV contribution to daily daytime ozone variation changed to negative values during the episode
316 period, which did not determine the trend of the DDOC. By comparing the accumulative effect of individual process to
317 the combined effect of the four processes (TOTAL_SUMs), the variation of DDOC (which increase from July 5 to 9
318 and decrease on July 10), was determined by the integrated effect of four processes, but mainly dominated by the
319 TOTAL_SUM_ADV (suddenly change from negative values to large positive values during episode).

320 The VMIX effect links the ground ozone variation to the ozone variation in the upper PBL level, which is dependent
321 on the vertical gradient of the concentration and the turbulence exchange coefficients (Gao et al. 2020). To understand
322 the connection and why the VMIX contribution to the surface ozone reach the maximum (131.0915ppb) from July 6 to
323 7, the vertical profiles of accumulative CHEM, ADV, CONV and CAC (CHEM+ADV+CONV) to the TOTAL_SUM
324 during the time period from 08:00 to 20:00 on July 5 -7 are shown in Fig. 8. (For example, the accumulative of CHEM
325 effect from 08:00 to 20:00 on July 6 is denoted as sum of CHEM 06_08-20).

326 The gradient of vertical profile of accumulative CHEM contribution on July 6 was significantly larger than that of
327 vertical profiles of accumulative CHEM contribution on July 5 and 7 (Fig. 8a). The CHEM increase in PBL is due to
328 the impact of the periphery of Typhoon, which would produce a field of meteorological conditions conducive to

329 photochemical reactions. These meteorological conditions also increased the absolute contribution and gradient of
 330 accumulative ADV contribution compared to that of July 5 (Fig. 8b). Therefore, the vertical profile gradient of sum of
 331 CVC 06_08-20 was the largest, which contributed to the enhancement of VMIX contribution to the ozone on the
 332 ground. In short, both the daytime CHEM and ADV enhancement above the ground throughout the PBL have
 333 contributed to the increase in VMIX contribution to the ground-level ozone. The CHEM enhancement above the
 334 ground throughout the PBL is due to the increase in photochemical formations of precursors, while the ADV
 335 enhancement above the ground throughout the PBL is attributed to the WWD (weak wind deepening) effect in the
 336 whole lower troposphere during the episode.

337



338

339 **Figure 8.** The vertical profiles of accumulative (a) CHEM, (b) ADV, (c) CONV, and (d) CVC (CHEM+ADV+CONV) during the periods

340

from 08:00 to 20:00 on July 5-7.

341 In summary, under the influence of the peripheral subsidence of typhoon, the weak subsidence associated with typhoon
 342 periphery bring clear sky and warmer air, which is conducive for the ozone photolysis formation (CHEM) above the
 343 ground in planetary boundary layer (PBL) and compensates the ozone through the positive VMIX effects on the
 344 ground. Therefore, the chemical formation (CHEM) and vertical mixing (VMIX) effects are two major contributors to
 345 forming TCs-Ozone episodes, while the ADV and CONV show negative values. However, the day-to-day daytime
 346 ozone levels do not associate with daily variation of daytime CHEM and VMIX, but dominated by the daily variation

347 of ADV (e.g., weakened advection outflow or dispersion). The daily enhanced ADV during the episode on the ground
348 and throughout the PBL is attributable to the WWD, which is a common phenomena induced by the peripheral
349 circulation of typhoon system. In addition, both the enhanced CHEM and ADV above the ground contribute to the
350 daily daytime ozone enhancement on the ground via the VMIX process during the episode.

351 **4. Conclusions**

352 In this study, the analysis of ground observation, wind profile data, and model simulation were integrated. By
353 analysing the wind profile radar observations, we found that not only surface weak winds but also WWD generally
354 appeared in the periphery of Typhoon. The statistics of wind fields and ground-level ozone at 7 wind profile radar
355 stations in PRD during the 38 typhoons in the Northwestern Pacific Ocean from 2014-2018 showed that the number of
356 WWD occurrences accounted for 93% (87-97%) of the available number of radar stations for the seven radar stations
357 in average. The number of ozone pollution occurrences accounted for 94% of the number of WWD occurrences in
358 average. The statistical results show that WWD is a common weather phenomenon in the periphery of typhoons
359 associated with periphery subsidence of typhoon system and is often accompanied by significant increases in ozone
360 concentrations.

361 The WRF-chem model was used to simulate the daily daytime ozone variation in a sustained ozone pollution process
362 in PRD during Typhoon Nepartak in 2016. Validation results showed that the model could reasonably reproduce the
363 observed temperature, wind speed, wind direction, and ozone. Process analysis results showed that under the impact of
364 the peripheral subsidence of typhoon, the chemical formation (CHEM) and vertical mixing (VMIX) effects are two
365 major contributors to the enhancement of ozone levels to form an episode, while the ADV and CONV always show
366 negative or small values. However, the day-to-day variation of the daytime ozone levels are not determined by the
367 daily variation of daytime CHEM, but are dominated by the daily variation of ADV terms on the ground (e.g. the
368 weakened advection outflow or dispersion) .So, the ozone and its precursors accumulation, including the enhancement

369 during the nighttime, contribute to the daytime ozone increase in the following day. Via a detailed day-to-day analysis,
370 we found that the decrease of negative ADV values during the event not only occurred on the ground but also
371 throughout the PBL. The daily enhanced VMIX contribution to the ground-level daytime ozone during episode is
372 associated with the enhanced CHEM and ADV in the upper PBL. Results show that in addition to the weakened
373 advection outflow or dispersion on the ground, the integrated effect of the day-to-day variation of the accumulative
374 CHEM above the ground and accumulative ADV contribution throughout the PBL determined together the overall
375 day-to-day daytime ozone variation through the VMIX process on the ground.

376 This study reveals that the peripheral characteristics of approaching typhoon not only form the ozone episode by the
377 enhanced photochemical reactions but also the change the day-to-day ozone levels by the pollution accumulation
378 throughout the PBL due to the weak wind deepening up to 3-5 km. This result explains the continues increase in
379 daytime ozone, although the photochemical contribution began to decrease during the event. It also reveals the
380 important role of WWD in the lower troposphere for the formation of sustained ozone episodes due to the peripheral
381 circulation of the typhoon, which helps to better predict the daily changes of daytime ozone levels.

382

383 *Author contributions.* Conceptualization, YL; methodology YL and XZ. JG performed model simulations. XZ and YL
384 analysed data and interpreted results. XZ, YL and XD have discussed the results and commented on the paper. XZ
385 wrote the paper with input from all co-authors.

386

387 *Competing interests.* The authors declare that they have no conflict of interest.

388

389 *Acknowledgements.* We would like to acknowledge the National Centers for Environmental Prediction (NCEP) for
390 the Final Operational Global Analysis data which are freely obtained from the website
391 <https://rda.ucar.edu/datasets/ds083.2/>. The hourly ambient surface O₃ concentration are real-timely released by
392 Ministry of Environmental Protection, China on the website <http://www.aqistudy.cn/>, freely downloaded from
393 <http://106.37.208.233:20035/>. The meteorological datas, such as the wind profiler data, automatic weather station data,
394 cloud data and so on, were provided by the China Meteorological Administration and downloaded from
395 <http://172.22.1.175>. This work was supported by National Natural Science Foundation of China (Grant no.
396 41961160728, 41575106), Shenzhen Science and Technology Program (KQTD20180411143441009); Key-Area
397 Research and Development Program of Guangdong Province (2020B1111360001), the Guangdong Basic and Applied
398 Basic Research Fund Committee (2020B1515130003), the NSFC/RGC (Grant No N_HKUST638/19), Key Special
399 Project for Introduced Talents Team of Southern Marine Science and Engineering Guangdong Laboratory (Guangzhou),
400 grant number GML2019ZD0210, The Guangdong Province Science and Technology Planning Project of China (Grant

401 no. 2017A050506003), Shenzhen Key Laboratory Foundation (ZDSYS20180208184349083), Center for
402 Computational Science and Engineering at Southern University of Science and Technology.

403

404

405

406 ■ **References**

- 407 Aunan, K., Berntsen, T. K., and Seip, H. M.: Surface Ozone in China and its Possible Impact on
408 Agricultural Crop Yields, *AMBIO J. Hum. Environ.*, 29, 294–301, 2000.
- 409 Chan, A., Fung, J. C. H., and Lau, A. K. H.: Influence of urban morphometric modification on regional
410 boundary-layer dynamics, *J. Geophys. Res. Atmospheres*, 118, 2729–2747, 2013.
- 411 Chen, X. L., Fan, S. J., Jiang-Nan, L. I., Ji, L., Wang, A. Y., and Soi-Kun, F.: typical weather
412 characteristics associated with air pollution in Hong Kong area, *J. Trop. Meteorol.*, 014, 101–104, 2008.
- 413 Chen, Z., Zhuang, Y., Xie, X., Chen, D., Cheng, N., Yang, L., and Li, R.: Understanding long-term
414 variations of meteorological influences on ground ozone concentrations in Beijing During 2006-2016.,
415 *Environ. Pollut.*, 245, 29–37, 2018.
- 416 Cheng, N. L., Li, Y. T., Zhang, D. W., Chen, T., Wang, X., Huan, N., Chen, C., and Meng, F.:
417 Characteristics of Ozone over Standard and Its Relationships with Meteorological Conditions in Beijing
418 City in 2014, *Environ. Sci.*, 37, 2016.
- 419 Deng, T., Wang, T., Wang, S., Zou, Y., Yin, C., Li, F., Liu, L., Wang, N., Song, L., and Wu, C. and:
420 Impact of typhoon periphery on high ozone and high aerosol pollution in the Pearl River Delta region,
421 *Sci. Total Environ.*, 668, 617–630, 2019.
- 422 Doll, D. C.: *Guideline for Regulatory Application of the Urban Airshed Model*, 1991.
- 423 Emery, C., Tai, E., and Yarwood, G.: Enhanced meteorological modeling and performance evaluation
424 for two texas episodes, in: Prepared for the Texas Natural Resource Conservation Commission, by
425 Environ International Corp, 2007.
- 426 Felzer, B. S., Cronin, T., Reilly, J. M., Melillo, J. M., and Wang, X.: Impacts of ozone on trees and crops,
427 *Comptes Rendus Géoscience*, 339, 784–798, 2007.
- 428 Feng, Y., Wang, A., Wu, D., and Xu, X.: The influence of tropical cyclone Melor on PM(10)
429 concentrations during an aerosol episode over the Pearl River Delta region of China: Numerical
430 modeling versus observational analysis, *Atmos. Environ.*, 41, p.4349-4365, 2007.
- 431 Feng, Z., Hu, E., Wang, X., Jiang, L., and Liu, X.: Ground-level O₃ pollution and its impacts on food
432 crops in China: A review, *Environ. Pollut.*, 199, 42–48, 2015.
- 433 Forkel, R., Werhahn, J., Hansen, A. B., Mckeen, S., Peckham, S., Grell, G., and Suppan, P.: Effect of
434 aerosol-radiation feedback on regional air quality – A case study with WRF/Chem, *Atmos. Environ.*, 53,
435 202–211, 2012.
- 436 Gao, J., Zhu, B., Xiao, H., Kang, Hou, X., and Shao, P.: A case study of surface ozone source
437 apportionment during a high concentration episode, under frequent shifting wind conditions over the
438 Yangtze River Delta, China, *Sci. Total Environ.*, 544, 853–863, 2016.
- 439 Gao, J., Zhu, B., Xiao, H., Kang, H., Hou, X., Yin, Y., Zhang, L., and Miao, Q.: Diurnal variations and
440 source apportionment of ozone at the summit of Mount Huang, a rural site in Eastern China, *Environ.*
441 *Pollut.*, 222, 513–522, 2017.

442 Gao, J., Li, Y., Zhu, B., Hu, B., Wang, L., and Bao, f.: What have we missed when studying the impact
443 of aerosols on surface ozone via changing photolysis rates?, *Atmospheric Chem. Phys.*, 10831-10844,
444 2020.

445 Giorgi, F. and Meleux, F.: Modelling the regional effects of climate change on air quality, *Comptes*
446 *Rendus Geosci.*, 339, 721–733, 2007.

447 Grell, G. A., Peckham, S. E., Schmitz, R., Mckeen, S. A., Frost, G., Skamarock, W. C., and Eder, B.:
448 Fully coupled “online” chemistry within the WRF model, 2005.

449 Han, H., Liu, J., Shu, L., Wang, T., and Yuan, H.: Local and synoptic meteorological influences on daily
450 variability of summertime surface ozone in eastern China, *Atmospheric Chem. Phys.*, 1–51, 2019.

451 Hu, J., Chen, J., Ying, Q., and Zhang, H.: One-Year Simulation of Ozone and Particulate Matter in
452 China Using WRF/CMAQ Modeling System, *Atmospheric Chem. Phys. Discuss.*, 16, 10333–10350,
453 2016.

454 Huang, J., Liu, H., Crawford, J. H., Chan, C., Considine, D. B., Zhang, Y., Zheng, X., Zhao, C., Thouret,
455 V., and Oltmans, S. J.: Origin of springtime ozone enhancements in the lower troposphere over Beijing:
456 in situ measurements and model analysis, 15, 5161–5179, 2015.

457 Jiang, Y. C., Zhao, T. L., Liu, J., Xu, X. D., Tan, C. H., Cheng, X. H., Bi, X. Y., Gan, J. B., You, J. F.,
458 and Zhao, S. Z.: Why does surface ozone peak before a typhoon landing in southeast China?,
459 *ATMOSPHERIC Chem. Phys.*, 15, 13331–13338, 2015.

460 Kwok, R. H. F., Fung, J. C. H., Lau, A. K. H., and Fu, J. S.: Numerical study on seasonal variations of
461 gaseous pollutants and particulate matters in Hong Kong and Pearl River Delta Region, *J. Geophys. Res.*
462 *Atmospheres*, 115, 2010.

463 Lai, L. Y. and Sequeira, R.: Visibility degradation across Hong Kong: its components and their relative
464 contributions, *Atmos. Environ.*, 35, 5861–5872, 2001.

465 Li, J., Wang, Z., Akimoto, H., Gao, C., Pochanart, P., and Wang, X.: Modeling study of ozone seasonal
466 cycle in lower troposphere over east Asia, *J. Geophys. Res. Atmospheres*, 112, 2007.

467 Li, Y., Lau, A. K. H., Fung, J. C. H., Ma, H., and Tse, Y.: Systematic evaluation of ozone control
468 policies using an Ozone Source Apportionment method, *Atmos. Environ.*, 76, 136–146,
469 <https://doi.org/10.1016/j.atmosenv.2013.02.033>, 2013.

470 Li, Y., Lau, A., Wong, A., and Fung, J.: Decomposition of the wind and nonwind effects on observed
471 year-to-year air quality variation, *J. Geophys. Res. Atmospheres*, 119, 6207–6220, 2014.

472 Li, Y., A. K.-H. Lau, J. C.-H. Fung, J. Y. Zheng, L. J. Zhong, and P. K. K. Louie, Ozone source apportionment (OSAT)
473 to differentiate local regional and super-regional source contributions in the Pearl River Delta region, China, *J.*
474 *Geophys. Res. Atmos.*, 117 (D15), 2012.

475 Li, T. Y., Deng, X. J., Li, Y., Song, Y. S., Li, L. Y., Tan, H. B., & Wang, C. L.. Transport paths and
476 vertical exchange characteristics of haze pollution in Southern China. *Science of the Total Environment*,
477 625, 1074-1087, 2018.

478

479 Lin, X., Yuan, Z., Yang, L., Luo, H., and Li, W.: Impact of Extreme Meteorological Events on Ozone in
480 the Pearl River Delta, China, *Aerosol Air Qual. Res.*, 19, 1307–1324,
481 <https://doi.org/10.4209/aaqr.2019.01.0027>, 2019.

482 Liu, J., Wu, D., Fan, S. J., Liao, Z. H., and Deng, T.: Impacts of precursors and meteorological factors
483 on ozone pollution in Pearl River Delta, *Zhongguo Huanjing Kexuechina Environ. Sci.*, 37, 813–820,
484 2017.

485 Lu, R., Turco, R. P., and Jacobson, M. Z.: An integrated air pollution modeling system for urban and
486 regional scales: 2. Simulations for SCAQS 1987, *J. Geophys. Res. Atmospheres*, 102, 6081–6098,
487 <https://doi.org/10.1029/96JD03502>, 1997.

488 Ministry of Ecology and Environment of China: Chinese State of the Environment Bulletin, 1–54, 2016.

489 Organization, W. H.: WHO Air quality guidelines for particulate matter, ozone, nitrogen dioxide and
490 sulfur dioxide - Global update 2005, 2005.

491 Shu, L., Xie, M., Wang, T., Gao, D., Chen, P., Han, Y., Li, S., Zhuang, B., and Li, M.: Integrated studies
492 of a regional ozone pollution synthetically affected by subtropical high and typhoon system in the
493 Yangtze River Delta region, China, *Atmospheric Chem. Phys.*, 16, 15801–15819, 2016.

494 Shu, L., Wang, T., Xie, M., Li, M., Zhao, M., Zhang, M., and Zhao, X.: Episode study of fine particle
495 and ozone during the CAPUM-YRD over Yangtze River Delta of China: Characteristics and source
496 attribution, *Atmos. Environ.*, 203, 87–101, <https://doi.org/10.1016/j.atmosenv.2019.01.044>, 2019.

497 Skamarock, W. C., Klemp, J. B., Dudhia, J., Gill, D. O., Barker, D. M., Duda, M. G., Huang, X.-Y.,
498 Wang, W., and Powers, J. G.: A Description of the Advanced Research WRF Version 3, 125, n.d.

499 Tan, Z., Lu, K., Jiang, M., Su, R., Dong, H., Zeng, L., Xie, S., Tan, Q., and Zhang, Y.: Exploring ozone
500 pollution in Chengdu, southwestern China: A case study from radical chemistry to O₃-VOC-NO_x
501 sensitivity, *Sci. Total Environ.*, 636, 775–786, 2018.

502 Wang, N.: Guangdong Haze Weather Bulletin, 21 pp., 2017.

503 Wang, T., Lam, K. S., Lee, A. S. Y., Pang, S. W., and Tsui, W. S.: Meteorological and Chemical
504 Characteristics of the Photochemical Ozone Episodes Observed at Cape D’Aguilar in Hong Kong, *J.*
505 *Appl. Meteorol.*, 37, 1167–1178, 1998.

506 Wang, T., Wu, Y. Y., Cheung, T. F., and Lam, K. S.: A study of surface ozone and the relation to
507 complex wind flow in Hong Kong, *Atmos. Environ.*, 35, 3203–3215, 2001.

508 Wang, X., Zhang, Y., Hu, Y., Zhou, W., and Russell, A. G.: Process analysis and sensitivity study of
509 regional ozone formation over the Pearl River Delta, China, during the PRIDE-PRD2004 campaign
510 using the CMAQ model, *Atmospheric Chem. Phys. Discuss.*, 9, 635–645, 2009.

511 Wang, Z., Li, J., Wang, X., Pochanart, P., and Akimoto, H.: Modeling of Regional High Ozone Episode
512 Observed at Two Mountain Sites (Mt. Tai and Huang) in East China, *J. Atmospheric Chem.*, 55,
513 253–272, 2006.

514 Wu, D., Tie, X., Li, C., Ying, Z., Lau, K. H., Huang, J., Deng, X., and Bi, X.: An extremely low
515 visibility event over the Guangzhou region: A case study, *Atmos. Environ.*, 39, p.6568-6577, 2005.

- 516 Wu, M., Wu, D., Fan, Q., Wang, B. M., Li, H. W., and Fan, S. J.: Observational studies of the
517 meteorological characteristics associated with poor air quality over the Pearl River Delta in China,
518 *Atmospheric Chem. Phys.*, 13, 10755–10766, <https://doi.org/10.5194/acp-13-10755-2013>, 2013.
- 519 Zaveri, R. A. and Peters, L. K.: A new lumped structure photochemical mechanism for large-scale
520 applications, *J. Geophys. Res. Atmospheres*, 104, 30387–30415, 1999.
- 521 Zaveri, R. A., Easter, R. C., Fast, J. D., and Peters, L. K.: Model for Simulating Aerosol Interactions and
522 Chemistry (MOSAIC), *J. Geophys. Res. Atmospheres*, 113, 2008.
- 523 Zhang, H., DeNero, S. P., Joe, D. K., Lee, H.-H., Chen, S.-H., Michalakes, J., and Kleeman, M. J.:
524 Development of a Source Oriented version of the WRF- Chem Model and its Application to the
525 California Regional PM10/PM2.5 Air Quality Study, 20, 2014.
- 526 Zhang, J. and Rao, S. T.: The Role of Vertical Mixing in the Temporal Evolution of Ground-Level
527 Ozone Concentrations, *J. Appl. Meteorol.*, 38, 1674–1691, 1999.
- 528 Zhang, J. P., Zhu, T., Zhang, Q. H., Li, C. C., Shu, H. L., Ying, Y., Dai, Z. P., Wang, X., Liu, X. Y., and
529 Liang, A. M.: The impact of circulation patterns on regional transport pathways and air quality over
530 Beijing and its surroundings, *Atmospheric Chem. Phys.*, 12, 5031–5053, 2012.
- 531 Zhang, Y., Wen, X. Y., and Jang, C. J.: Simulating chemistry-aerosol-cloud-radiation-climate feedbacks
532 over the continental U.S. using the online-coupled Weather Research Forecasting Model with chemistry
533 (WRF/Chem), *Atmos. Environ.*, 44, p.3568-3582, 2010.
- 534 Zhang, Y., Mao, H., Ding, A., Zhou, D., and Fu, C.: Impact of synoptic weather patterns on
535 spatio-temporal variation in surface {O₃} levels in Hong Kong during 1999–2011, *Atmos. Environ.*, 73,
536 41–50, 2013.
- 537 Zhu, B., Kang, H., Zhu, T., Su, J., Hou, X., and Gao, J.: Impact of Shanghai urban land surface forcing
538 on downstream city ozone chemistry: URBAN LAND-SURFACE FORCING ON OZONE, *J. Geophys.*
539 *Res. Atmospheres*, 120, 4340–4351, <https://doi.org/10.1002/2014JD022859>, 2015.
- 540 Ziomas, I. C., Melas, D., Zerefos, C. S., Bais, A. F., and Paliatsos, A. G.: Forecasting peak pollutant
541 levels from meteorological variables, *Atmos. Environ.*, 29, 3703–3711, 1995.

542
543